Identifying reservoir depletion patterns from production-induced deformations with applications to seismic imaging

Musa Maharramov

ABSTRACT

The ultimate objective of our research is to study the feasibility of using subsidence measurements for the regularization of linearized waveform inversion of time-lapse data sets, and for differential travel-time tomography. In this paper, we focus on developing a robust framework for inverting pore pressure change in a production reservoir from partial displacement or subsidence data, and on estimating subsurface displacements from the inverted pore pressure change. We discuss potential applications of the resulting displacement fields to the estimation of production-induced change of seismic velocities and impedance. Sensitivity of the proposed framework to the uncertainty and spatial heterogeneity of the poroelastic subsurface parameters is discussed as well.

INTRODUCTION

Our objective is to study the application of geological and geomechanical constraints to the regularization of seismic inversion problems. Well tie-ins and use of a priori information on sediment geometry are examples of such constraints that have found robust quantitative application in regularized seismic inversion. Although some success has been achieved in attempts to connect subsurface velocities and impedance to poroelastic rock properties (Mavko et al., 2009), the application of such relations to constraining velocity inversion runs into difficulties stemming from uncertainties both in the subsurface parameters and in the choice of a semi-empirical rock model to use. However, displacement and stress measurements are the source of independent information about the subsurface, and in principle may be used for the regularization of seismic inversion problems in areas of poor illumination.

More specifically, in the framework of time-lapse seismic imaging, we are interested in answering the following two questions:

- Can we robustly estimate production-induced changes in seismic velocities and impedance (with respect to a base-line model) from subsidence measurements?
- Can we subsequently use the updated model for the regularization of time-lapse inversion where repeat surveys have illumination gaps or are contaminated with noise?

While we discuss the second question in the penultimate section, this paper is mostly concerned with the first question. We begin with an overview of the existing theory of production-induced deformation, then proceed to the formulation of our method for modeling displacements from known pressure drop in a "slowly varying" poroelastic medium. A technique for inverting the pore pressure change from measured displacements is described next. The proposed modeling and inversion techniques are demonstrated on synthetic examples based on real-world production-induced subsidence cases. The section on spatial heterogeneity of elastic earth models discusses the impact of heterogeneity on modeling and inversion results and puts forward an extension of the proposed technique for tackling vertically-layered and arbitrarily heterogeneous media. The paper concludes with a discussion of velocity and impedance change estimation from strain, with an outline of a process for picking the appropriate semi-empirical rock model.

PRODUCTION-INDUCED DEFORMATION

Realistic reservoir depletion exhibits *asymmetric* patterns that might be indicative of a complex reservoir geometry as well as spatial heterogeneity of the reservoir permeability. In particular, differences in production-related pressure change across multiple wells can help identify reservoir compartmentalization (Zoback, 2010) and guide the drilling of subsequent production wells, or affect the choice of production-enhancement techniques. In the general case of an arbitrary linear poroelastic medium, change in the pore pressure is intricately interconnected with the change in the stress field, and accurate modeling of the effects of changing pore pressure requires solving a system of governing equations in a half-space (Wang, 2000), (Segall, 2010). Solving a boundary-value problem for such a system of equations governing both stress evolution and fluid flow is challenging – as much due to uncertainty of the subsurface model parameters as due to the sheer analytical complexity of these coupled equations. The importance of studying the fully-coupled poroelastic models cannot be overestimated as the coupled modeling is often the key to explaining counterintuitive behaviour of some real-world poroelastic models.

In this work we expand on previous studies of the effects of pore pressure change on the strain and stress fields (Segall, 1992),(Segall et al., 1994) by adopting an intermediate approach between the fully coupled simulation and uncoupled analytical solutions. First, we assume that a pore pressure drop is known within the reservoir and is an arbitrary function of the reservoir coordinates – i.e., we assume partial *fluid-to-solid* coupling – and use the analytical expression for the elastostatic Green's tensor due to a concentrated centre of dilatation in half-space (Segall, 2010),(Mindlin, 1936) to *numerically compute* the displacement due to the pore pressure change. Next, we use the obtained numerical operator in an inversion problem, fitting a pore pressure drop to a known displacement and subsidence profile. Finally, we extend the method for layered media. The method is demonstrated on synthetic data based on a real-world example of subsidence due to the production from a hydrocarbon

reservoir at Lacq, France (Segall et al., 1994). Extensions of this study to joint application with time-lapse seismic imaging are discussed as well. This paper is dedicated to reporting some geomechanical aspects of the joint geomechanics/seismic imaging effort aimed at applying the author's optimisation framework to problems of computational geophysics.

As a side note, apart from its *potential* application to the regularization of seismic inversion, numerical modeling of deformation due to changing pore pressure is one of the key problems of reservoir geomechanics (Zoback, 2010). Reservoir depletion has been demonstrated to have appreciable effect on stress both inside and outside of the producing reservoir (Zoback, 2010),(Geertsma, 1973),(Segall, 1992),(Segall et al., 1994),(Zoback and Zinke, 2002),(Segall and Fitzgerald, 1998). While some simplifying assumptions with regard to reservoir geometry (e.g., an infinitely wide and thin horizontal layer) yield a simple law for the horizontal stress change with the pressure decline *within the reservoir* (Zoback, 2010),(Segall and Fitzgerald, 1998)), estimating induced stress-field changes around the reservoir requires more elaborate models of reservoir depletion (Geertsma, 1973),(Segall, 1992). Simple disk-shaped and radially-symmetric reservoir shapes proved adequate for many simple situations, but compartmentalization and heterogeneous permeability inside realistic reservoirs point to a departure of the pore pressure decline from simple axisymmetric patterns (Zoback, 2010). Compartmentalization with impermeable barriers still allows for the application of a radially-symmetric pore pressure change law to individual reservoir compartments. However, an asymmetric pore pressure drop should be able to account for the effects of partial permeability or complex spatial geometry. Since a computationally-efficient technique for modeling and inverting asymmetric reservoir depletion patterns is an important by-product of our study, it is hoped that the computational tools and methods developed for this study will find independent application to the study of production-induced stressing and deformation.

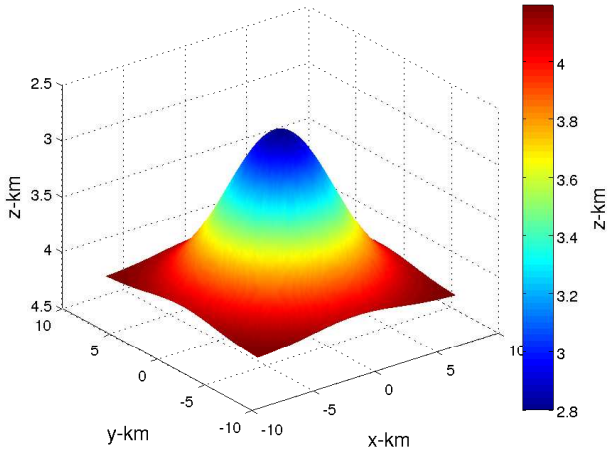

Figure 1: Reservoir dome. The effective depth of the reservoir is 3.5km, effective radius $\approx$ 8km and width $\approx$ .35 km. [**ER**]

GOVERNING EQUATIONS

We begin by formulating a *closed* system of four equations that describes a homogeneous *quasi-static* linear poroelastic medium (Segall, 2010):

$$\mu\nabla^2 u_i + \frac{\mu}{1-2\nu}\frac{\partial^2 u_j}{\partial x_i \partial x_j} = \alpha\frac{\partial p}{\partial x_i} - f_i = 0,\ i = 1,2,3 \tag{1}$$

and

$$S_\alpha \frac{\partial p}{\partial t} - \frac{\kappa}{\eta}\nabla^2 p = -\alpha\frac{\partial}{\partial t}\left(\nabla\cdot\mathbf{u}\right). \tag{2}$$

In the above equations $u_i, i = 1,2,3$ is a spatially-distributed *displacement* vector field, p is the *pore pressure change*, f_i is a differential body-force distribution, $\mu, \nu, \alpha, \kappa, \eta$ are the shear modulus, Poisson's ratio, Biot coefficient, permeability and fluid viscosity, respectively. The *storage coefficient* S_α is a known function of medium parameters (Segall, 2010):

$$S_\alpha = \frac{3\alpha(1-2\nu)(1-\alpha B)}{2\mu B(1+\nu)}, \tag{3}$$

where B in equation 3 is *Skempton's pore pressure coefficient* – the ratio of induced pore pressure to the mean normal stress for *undrained* loading conditions. Note that the *subsurface stress* is absent from equations 1,2 but can be computed using the constitutive laws after these equations have been solved. Also note that the displacement and pore pressure in these equations are *relative* to a reference state, not the total values. The equilibrium equation 1 and flow equation 2 are fully coupled and are obtained from combining the constitutive laws for a poroelastic medium with quasi-static field equations. The equations are "quasi-static" in the sense that the stress field is assumed to be in a state of static equilibrium even though changes of the pore pressure in time induce changes of the stress field. We can think of this as a "slow-change" asymptotic approximation, both in time and space.

The most "mathematically accurate" way of computing the displacement field and associated pore pressure change is to solve a boundary-value problem for 1,2 with known data (e.g., known pressure evolution within existing wells, measured earth displacements or estimated stresses) used as *boundary* or *initial* conditions. However, even in the simplest cases of a homogeneous medium, analytical solutions of boundary-value problems for equations 1,2 is challenging. *Uncoupling* equations 1 and 2, where permissible, could result in more tractable problems, both analytically and numerically. For example, assuming a known pore pressure change, we can solve equation 1 for the displacement field u_i, using $\alpha\frac{\partial p}{\partial x_i}$ in the right-hand side as a "body force" distribution (Geertsma, 1973),(Segall, 1992).

In our approach we use the elastostatic Green's tensor $g_i^k(x,y,z,\xi,\eta,\zeta)$ for the pure elastic equilibrium equation in the left-hand side of equation 1 to compute the displacement u_i as

$$u_i = -\alpha\int_V g_i^k\frac{\partial p}{\partial x_k} = \alpha\int_V \frac{\partial g_i^k(x,y,z,\xi,\eta,\zeta)}{\partial x_k}p(\xi,\eta,\zeta)d\xi d\eta d\zeta, \tag{4}$$

assuming $f_i = 0$ (including body forces is trivial). The elastostatic tensor $g_i^k(x, y, z, \xi, \eta, \zeta)$ in equation 4 has the meaning of the displacement along axis i at point (x, y, z) due to a concentrated force along axis k at point (ξ, η, ζ) (Wang, 2000),(Segall, 2010). From equation 4 we can see that the divergence of the elastostatic tensor has the meaning of deformation due to a concentrated dilatational force.

In order to apply equation 4 to practical reservoir models and computation of *surface subsidence*, the corresponding Green's function should be constructed for a *half-space* with the free-boundary condition imposed on its bounding plane (Segall, 2010). We use the analytical expression for the Green's function obtained by Mindlin (Mindlin, 1936) – see Appendix A for the details. The integral in the right-hand side of 4 is taken over the reservoir domain and hence singularities corresponding to $(x, y, z) = (\xi, \eta, \zeta)$ do not appear. However, the terms in non-diagonal tensor components that contain $r_2 - z - \zeta$ in the denominator blow up at locations directly above (or below) the reservoir and must be truncated in a numerical quadrature. Another important aspect of using an analytical expression for the Green's function is that the divergence in the right-hand side of equation 4 can be calculated analytically. However, in our implementation we compute the divergence using central differences of the second-order of accuracy.

MODELING DISPLACEMENTS FROM PORE-PRESSURE DECLINE

We can use operator 4 for forward-modeling the displacement field from a specified pressure change. Note that operator 4 is a non-stationary convolutional integral operator for a homogeneous medium. The convolution is non-stationary due to the presence of $z + \zeta$ in the elastostatic Green's tensor. Integration along the horizontal axes can be accelerated by applying the operator in the wavenumber domain. However, integration along the vertical axis should still be carried out separately for different values of z, hence the integration kernel is effectively four-dimensional. Assuming the reservoir to be thin in comparison with its lateral extents, which is always the case, we can replace the vertical integral with a mean value of the integrand times the reservoir thickness:

$$u_i(x, y, z) = \alpha \int_V h(\xi, \eta) \frac{\partial g_i^k(x, y, z, \xi, \eta, S(\xi, \eta))}{\partial x_k} p(\xi, \eta, S(\xi, \eta)) d\xi d\eta, \tag{5}$$

where $S(\xi, \eta)$ is the middle surface of the reservoir and $h(\xi, \eta)$ is the reservoir depth. For a non-flat reservoir, g_i^k effectively depends not only on differences $x - \xi$ and $y - \eta$ but on integration variables as well. In our implementation we compute 5 as a full convolutional operator, allowing *slowly-varying* asymptotics of the solutions by introducing scaling factors that depend on *both* (x, y, z) and (ξ, η, ζ).

An implementation of this method is provided by the `poroelastic_green.F90` module of the author's `exp_tk` Fortran 2003 object-oriented framework described in Appendix B.

We test our approach on synthetic data generated for a reservoir model based on the assumed geometry of the gas reservoir near Lacq, France, described by Segall et al. (1994). The reservoir is assumed to be anticlinal dome-shaped, with the depth of the reservoir approximated as

$$D(\rho) = 3.5 - 1.4\left(\exp\left[\left(\frac{\rho}{5}\right)^2\right] - .5\right), \tag{6}$$

where ρ is the distance to the center of the reservoir, and all the distances are measured in `km` (see Fig 1). The reservoir thickness is estimated to be $\approx .35$ `km`. In the first test we apply the forward-modeling operator 5 to an axisymmetric synthetic pore pressure drop similar to the pore pressure change used by Segall et al. (1994) and given by

$$p(\rho) = 55 \times \exp\left[\left(\frac{\rho}{8}\right)^4\right], \tag{7}$$

(see Fig 2(a)). The pressure in equation 7 and the rest of the paper is measured in `MPa`, and ρ is the distance to the center of the reservoir. The result of displacement modeling using an 81×81 reservoir grid and 101×101 surface grid is shown on Fig 2(b). Linear poroelasticity predicts a linear relationship between the maximum subsidence and the maximum pore pressure decline. Segall et al. (1994) predicts that the subsidence rate for the axisymmetric model is bracketed between .7 `mm/MPa` for the reservoir thickness of .25 `km` and 1.37 `mm/MPa` for the thickness of .45 `km`. The subsidence rate indicated by Fig 2(b) for the value of the reservoir thickness of .35 `km` is in a good agreement with that prediction. i

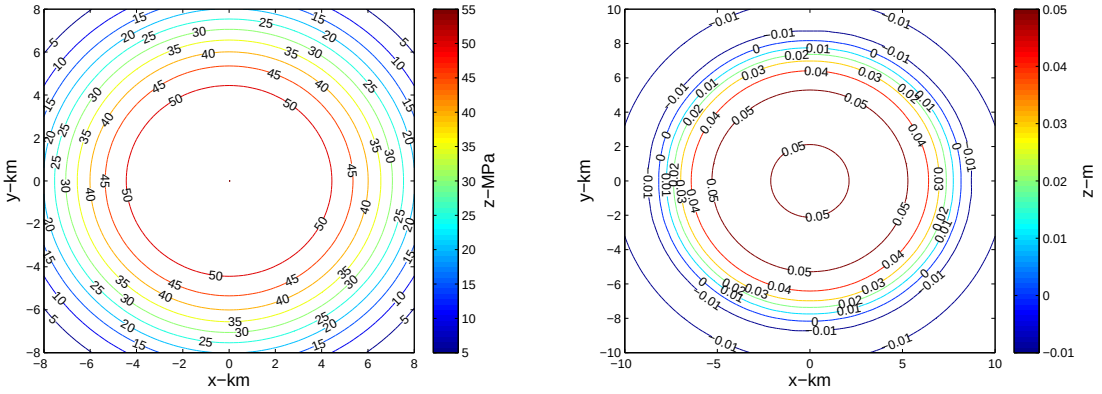

(a) (b)

Figure 2: a) Contour plot of the axisymmetric pore pressure drop given by equation 7. b) Contour plot of the subsidence above the reservoir of Fig 1 due to the axisymmetric pore pressure decline of Fig 2(a). [**ER**]

Next, we apply the modeling operator to the asymmetric synthetic pore pressure drop given by

$$p(\rho) = 55 \times \exp\left[\left(\frac{\rho}{8(1+\sin\phi - \pi/4)}\right)^4\right], \tag{8}$$

where ρ, ϕ are the distance and azimuth from an off-centre point (3 km,3 km), with a steeper decline in pore pressure along the northeast-southwest directions (see Fig 3(a)). The pressure decline given by equation 8 is not based on any specific real-world example but is rather chosen as a somewhat extreme case of an asymmetric pressure decline pattern mismatching the reservoir geometry. The result of modeling displacements due to the asymmetric pore pressure decline within the reservoir, using the same reservoir and surface grids as above, is shown on Fig 3(b).

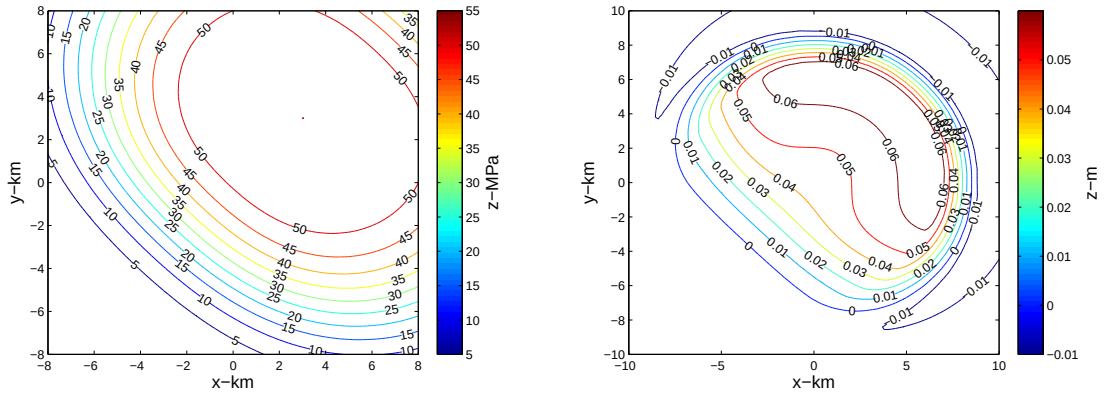

(a) (b)

Figure 3: a) Contour plot of the asymmetric pore pressure drop given by equation 8. b) Contour plot of the subsidence above the reservoir of Fig 1 due to the asymmetric pore pressure decline of Fig 3(a). [**ER**]

The following table summarizes the medium parameters taken from (Segall et al., 1994) that are used in our tests:

Parameter	SI	Imperial
ν	.25	dimensionless
α	.25	dimensionless
μ	23. GPa	3.34 Mpsi

The Biot coefficient α is computed as

$$\alpha = 1 - \frac{K_{\mathtt{und}}}{K_{\mathtt{min}}}, \tag{9}$$

with $K_{\mathtt{und}}, K_{\mathtt{min}}$ being the undrained bulk modulus and the bulk modulus of rock mineral grains, respectively (Mavko et al., 2009).

Modeling subsidence using operator 5, we are able to fully account for the asymmetric nature of the depletion pattern by using the most general form of Green's tensor for a homogeneous half-space. In that respect, our approach represents an advancement of the purely analytical techniques for axisymmetric reservoirs presented

in (Geertsma, 1973) and (Segall et al., 1994). However, the assumption of homogeneity, which is required for our being able to use analytical expressions for the Green's tensor, is a serious limitation that may significantly impair the applicability of our method, especially bearing in mind that our ultimate objective is to estimate subsurface displacements from observable subsidence. Later in the paper we propose a computationally efficient extension of our method that is capable of tackling heterogeneity.

ESTIMATING PORE-PRESSURE DECLINE FROM DISPLACEMENTS

Denoting the operator in the right-hand side of equation 5 as A, the problem of recovering the pore pressure decline from specified displacements can be cast as a least-squares minimisation problem:

$$\|Ap - u\|_{L_2} \quad \rightarrow \quad \min. \tag{10}$$

To solve 10 we use the object-oriented Fortran 2003 optimisation framework `exp_tk` developed by the author that implements multiple general-purpose optimisation methods. The implementation is fully decoupled from underlying model and data structures and can be used in a variety of applications. The tools described in Appendix B implement forward modeling and inversion, with the latter performed by applying a Krylov solver (Trefethen and Bau, 1997),(Bjork, 1996) with a user-specified number of iterations.

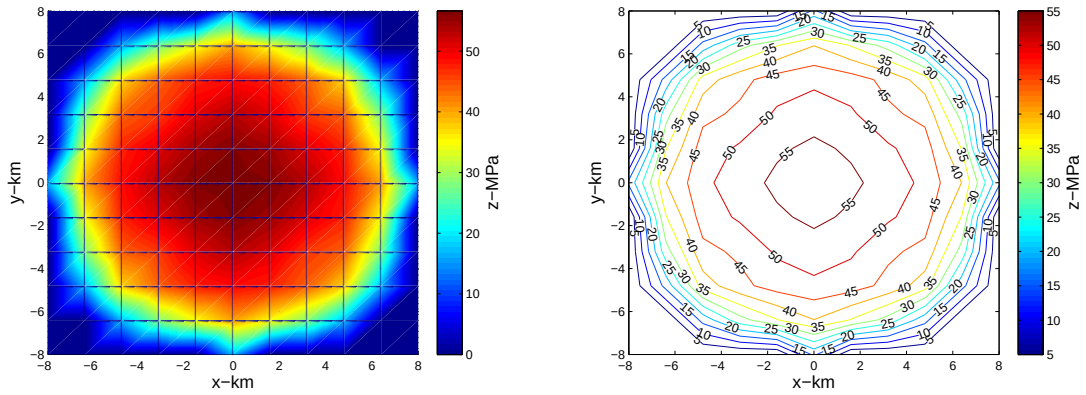

(a) (b)

Figure 4: a) Axisymmetric pore pressure decline inverted from the forward-modelled subsidence of Fig 2(b) on a sparse 11×11 grid after 4 solver iterations. b) Contour plot of the inverted axisymmetric pore pressure of Fig 4(a). [**ER**]

We test the inversion code first by inverting the previously modelled displacement for the axisymmetric and asymmetric pore pressure decline patterns of of Fig 2(a) and

3(a). Fig 4(a) and Fig 4(b) show the result for the axisymmetric pore pressure decline inverted on a sparse 11×11 grid in 4 iterations. We employ a *multigrid approach* (Iserles, 2008) where the inversion result obtained on a sparser grid is supplied as an initial approximation to the inversion on a denser grid. The inversion result for the 11×11 grid was supplied as an initial approximation to the pressure decline for the inversion on the denser 81×81 grid, and the resulting inverted axisymmetric pore pressure decline after 2 more iterations is shown on Fig 5(a) and Fig 5(b).

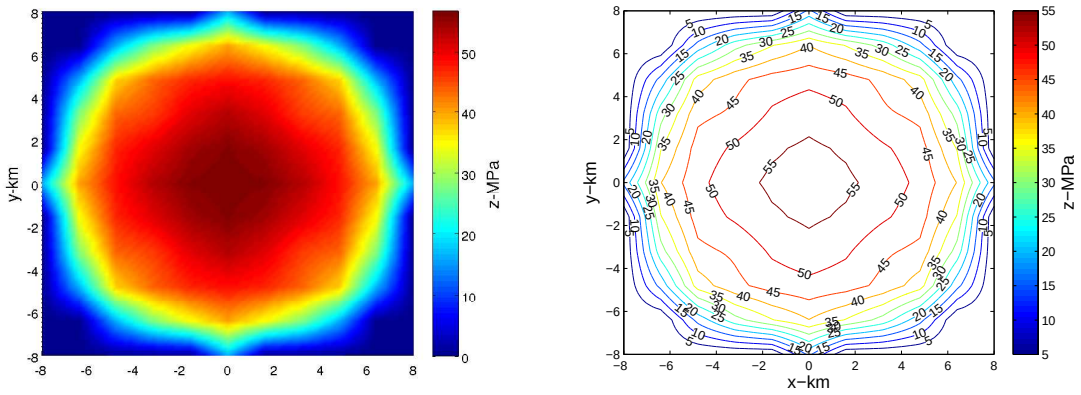

(a) (b)

Figure 5: a) Axisymmetric pore pressure decline inverted from the forward-modelled subsidence of Fig 2(b) on a denser 81×81 grid after 2 more solver iterations (total 6). b) Contour plot of the inverted axisymmetric pore pressure of Fig 5(a). [**ER**]

We have run a similar test for the asymmetric pore pressure decline of Fig 3(a) and equation 8. The result for the sparse grid and 5 iterations is shown on Fig 6(a) and Fig 6(b). The result of 2 more solver iterations on the denser grid is shown on Fig 7(a) and Fig 7(b).

Comparison of Fig 5(b) with Fig 2(a) and of Fig 7(b) with Fig 3(a) indicates a good agreement of the inverted pore pressure decline with the synthetics, violated mostly by the distortions near reservoir edges. Due to the least-squares problem being *ill-conditioned* for large data and model spaces, convergence on denser reservoir grids cannot be achieved without a good initial approximation. This issue has been successfully resolved by using the multigrid approach.

Note that although this test confirms the correct operation of our forward/inverse operator pair, by applying our inverse solver to the data modelled using the *underlying forward-modeling operator* we commit an *inversion crime*. True applicability of our method will be demonstrated in the next section where we apply it to a synthetic extrapolated from real subsidence data. While we are able to recover asymmetric pore pressure decline from as little data as can be contained in just *one* component of the measured displacement field, it is important to understand the sensitivity of our result to the *uncertainty* of the reservoir model parameters. Using operator 5 requires

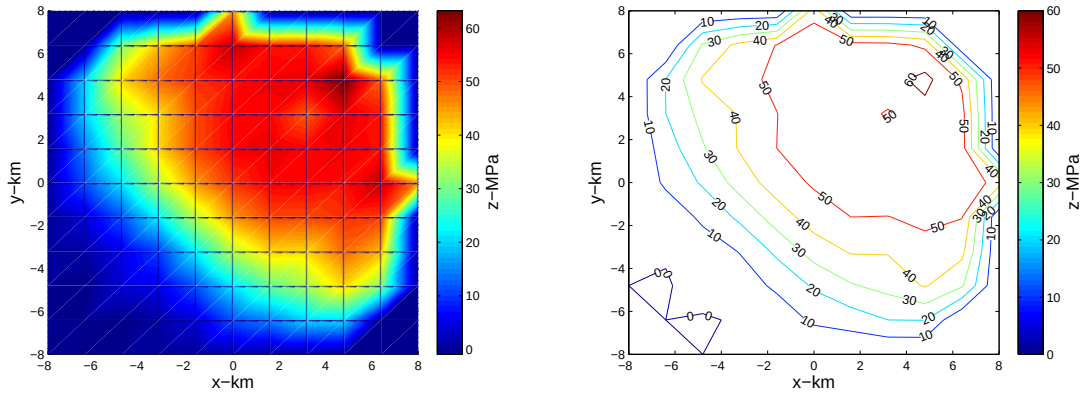

(a) (b)

Figure 6: a) Asymmetric pore pressure decline inverted from the forward-modelled subsidence of Fig 3(b) on a sparse 11×11 grid after 5 solver iterations. b) Contour plot of the inverted asymmetric pore pressure of Fig 6(a). [**ER**]

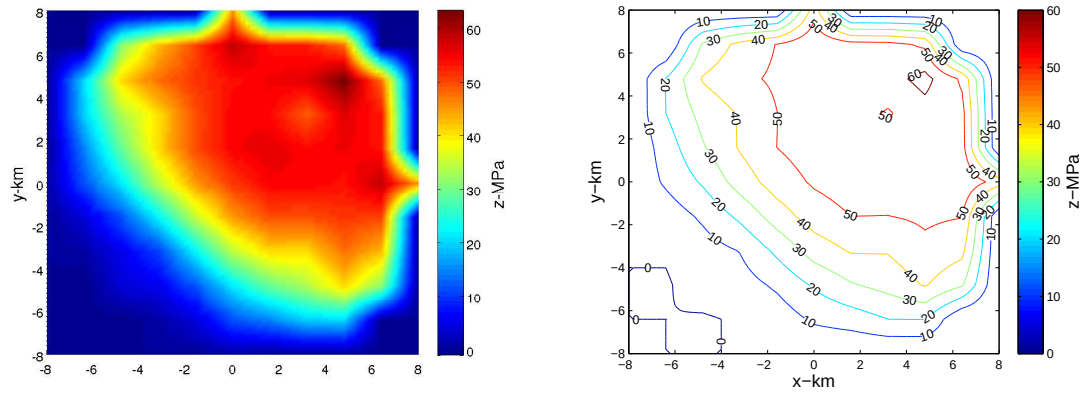

(a) (b)

Figure 7: a) Asymmetric pore pressure decline inverted from the forward-modelled subsidence of Fig 3(b) on a denser 81×81 grid after 2 more solver iterations (total 7). b) Contour plot of the inverted asymmetric pore pressure of Fig 7(a). [**ER**]

prior knowledge of medium and reservoir parameters, and using Mindlin's analytical expressions for elastostatic Green's tensor assumes *homogeneity* of the medium. In the numerical implementation of our method we effectively depart from the assumption of homogeneity by assuming instead *local* homogeneity or *slow* relative spatial change of medium parameters on the scales of reservoir length and depth. More precisely, our computational framework allows recasting operator 5 as

$$\mathbf{u}(x,y,z) \;=\; m(x,y,z)\mathbf{F}\left[r(\xi,\eta,\zeta)p(\xi,\eta,\zeta)\right] \tag{11}$$

where $\mathbf{F}$ is a homogeneous modeling operator, and $m(x,y,z)$ is a medium heterogeneity factor that, in the simplest case of slow-variability asymptotics (Maharramov, 2011),(Maslov, 1990),(Danilov et al., 1995), is equal to

$$m(x,y,z) = \frac{1}{\overline{\mu}(x,y,z)(1-\overline{\nu}(x,y,z))}, \tag{12}$$

where the overscore in equation 12 represents some average value of the corresponding medium parameter. The scaler r in the right-hand side of equation 11 is related to the heterogeneity of *reservoir* parameters, most notably the Biot coefficient. Equation 11 should include additional terms containing spatial derivatives of the Biot coefficient, but we ignore those terms under the assumption of mild spatial heterogeneity. Equation 11 suggests the following procedure for assessing the impact of the uncertainty in the values of the elastic moduli outside of the reservoir, assuming that r in equation 11 is 1 (i.e., reservoir parameters are integrated into F). The uncertainty of the pore pressure change due to a *concentrated* displacement $\delta(x-x_0, y-y_0, z-z_0)$ (along a fixed coordinate axis) is given by

$$\Delta p(\xi,\eta,\zeta) \;=\; \mathbf{F}^{-1}\left[\delta(x,y,z)\right] \times \Delta\frac{1}{m(x_0,y_0,z_0)}, \tag{13}$$

where the uncertainty $\Delta\frac{1}{m(x_0,y_0,z_0)}$ is computed from the associated uncertainties of the constituent medium parameters (e.g., moduli). Easy computation of the modeling operator and its inverse and the applicability of a multiscale/multigrid approach, as demonstrated in this paper, allow for a straightforward application of equation 13 to either estimating uncertainty or computing the *mathematical expectation* of the inverted pore pressure change.

APPLICATION TO EXTRAPOLATED LACQ SUBSIDENCE

In this section we describe the result of applying our inversion technique to estimating pore pressure decline from the measurements of subsidence for the reservoir described in Segall et al. (1994). Note that the subsidence data in (Segall et al., 1994) was one-dimensional, along the northwest-southeast line, so we extrapolated the data smoothly between the opposite azimuths (see Fig 8(a) and Fig 8(b)).

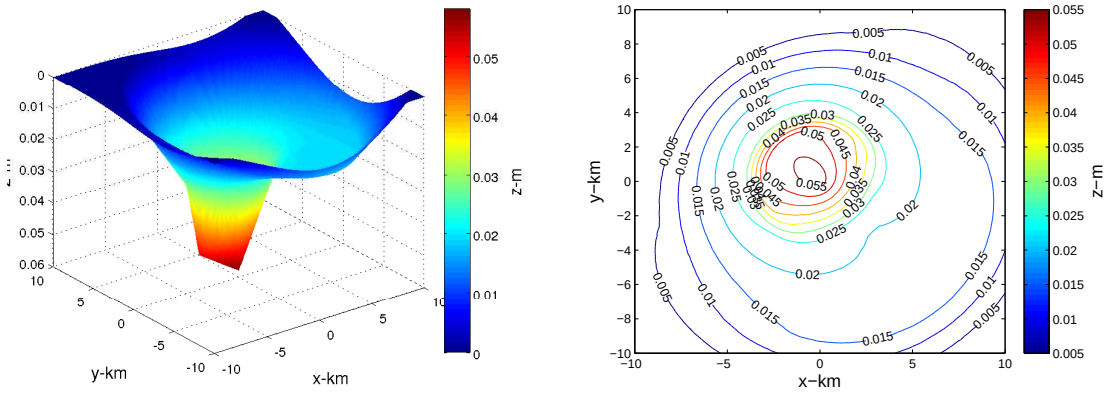

(a) (b)

Figure 8: a) Subsidence data from the Lacq reservoir, extrapolated onto a plane from northwest-southeast profile described in (Segall et al., 1994). b) Contour plot of Fig 8(a). [**ER**]

Since only the vertical displacement at the surface is known to us, we use the option of the inversion tool (see Appendix B) that constrains the modelled displacement components to just the vertical component. The result of running 2 iterations of our inversion algorithm on an 11×11 grid is shown on Fig 9(a),9(b). Results of the subsequent refinement in 2 more iterations over the 81×81 grid is shown on Fig 10(a),10(b).

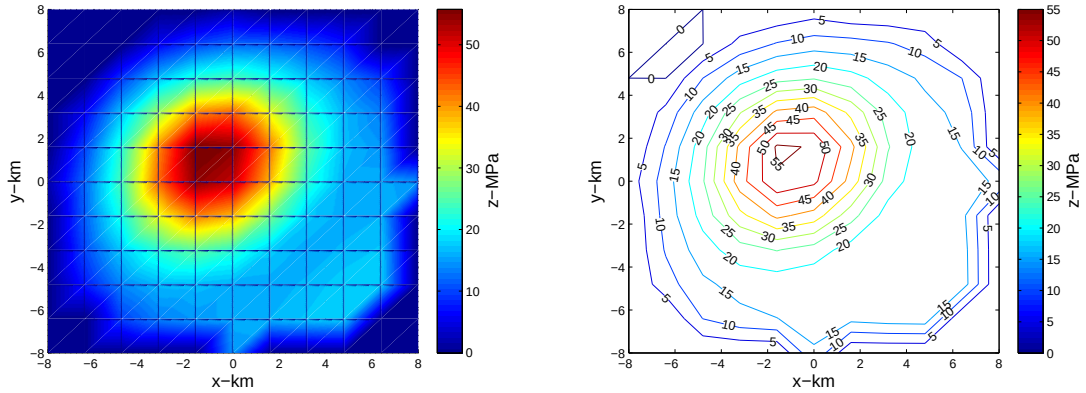

(a) (b)

Figure 9: a) Pore pressure decline inverted from the subsidence of Fig 8(b) on a sparse 11×11 grid after 2 solver iterations. b) Contour plot of the inverted pore pressure decline of Fig 9(a). [**ER**]

And finally, and most importantly, the symmetrized part of the reconstructed pore pressure drop is in excellent agreement with the input parameters of the *symmetric*

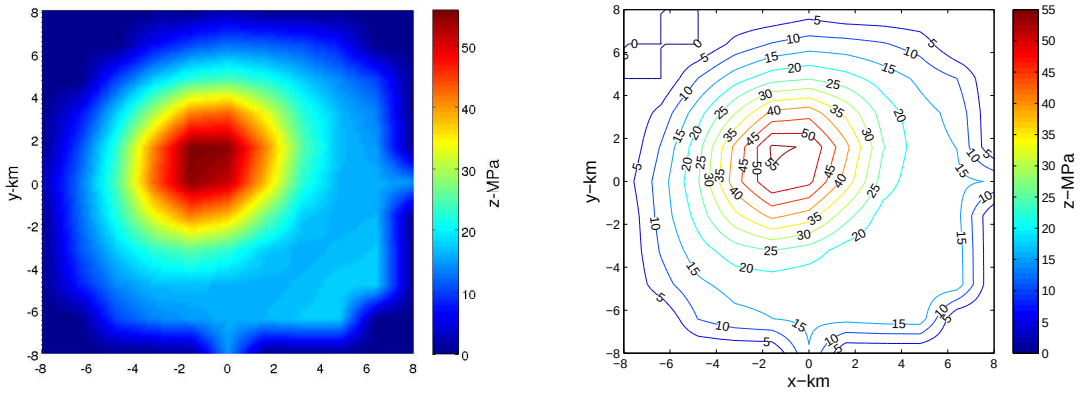

(a) (b)

Figure 10: a) Pore pressure decline inverted from the subsidence of Fig 8(b) on a denser 81×81 grid after 2 more solver iterations (total 4). b) Contour plot of the inverted pore pressure decline of Fig 10(a). [**ER**]

pore pressure profile used in (Segall et al., 1994) to (approximately) model the same subsidence data but using an *axisymmetric* pressure decline model. In particular, the peak pore pressure drop of 55 `MPa` at the end of the study period has been reconstructed precisely.

HETEROGENEOUS MODELS

Although the asymptotic technique discussed in an earlier section addresses to some extent the issue of inhomogeneous models, it is inherently limited to moderate heterogeneity. However, practical applications of this method would require a more accurate handling of heterogeneity. Because layered models are of particularly high importance due to their commonality, we first consider modeling displacements for a vertically heterogeneous and horizontally slowly-varying medium. Rather than trying to solve a heterogeneous analogue of system 1 and 2, we will assume that one or all components of the displacement at a fixed depth $z = z_{\max}$ immediately above the reservoir are known a priori. For example, we may use operator 5 to model displacements near the reservoir where the effect of the spatial heterogeneity of elastic parameters is limited. With displacements at $z = z_{\max}$ and free-surface boundary conditions at $z = 0$, the problem of modeling subsurface displacements is reduced to solving a boundary-value problem for the elastostatic system:

$$\begin{aligned} \mu\left(\frac{\partial u_i}{\partial x_j}+\frac{\partial u_j}{\partial x_i}\right)+\frac{2\mu\nu}{1-2\nu}\frac{\partial u_k}{\partial x_k}\delta_{ij} &= \sigma_{ij}, \\ \frac{\partial \sigma_{ij}}{\partial x_j} &= 0, \end{aligned} \tag{14}$$

where indices run from 1 to 3, σ_{ij} denote the *stress tensor* components, summation is carried out on repeating indices and body-force distribution is zero. The boundary conditions used with system 14 are the following:

$$\begin{aligned}\left(\frac{\partial u_i}{\partial x_3}+\frac{\partial u_3}{\partial x_i}\right)+\frac{2\nu}{1-2\nu}\frac{\partial u_k}{\partial x_k}\delta_{i3}|_{z=z_0} =&0,\\ u_i(x,y,z_{\mathrm{R}}) =&s_i(x,y),\end{aligned} \tag{15}$$

where $s_i(x,y),\ i=1,2,3$ is a known displacement field at a fixed depth. Although system 14 is comprized of purely elastostatic equations, it allows us to model fluid-to-solid coupling via the boundary condition at $z=z_{\mathrm{R}}$ that can be approximately computed using operator 5. For a laterally-homogeneous medium – or under the assumption of slow lateral variability and pseudo-differential operator ordering, (Maslov, 1976) – equations 14 can be Fourier-transformed in x_1, x_2, and the resulting system discretized in depth:

$$\begin{aligned}\frac{v_1(z+\Delta z)-v_1(z-\Delta z)}{2\Delta z} =&v_4(z)\\ \frac{v_2(z+\Delta z)-v_2(z-\Delta z)}{2\Delta z} =&v_5(z)\\ \frac{v_3(z+\Delta z)-v_3(z-\Delta z)}{2\Delta z} =&v_6(z)\\ \frac{\mu(z+\Delta z)v_4(z+\Delta z)-\mu(z-\Delta z)v_4(z-\Delta z)}{2\Delta z} =&\\ -(k_x^2+k_y^2+\frac{k_x^2}{1-2\nu(z)})\mu(z)v_1(z)-\frac{k_xk_y}{1-2\nu(z)}\mu(z)v_2(z)+\frac{ik_x}{1-2\nu}\mu(z)v_6(z)&\\ \frac{\mu(z+\Delta z)v_5(z+\Delta z)-\mu(z-\Delta z)v_5(z-\Delta z)}{2\Delta z} =&\\ -(k_x^2+k_y^2+\frac{k_y^2}{1-2\nu(z)})v_2(z)-\frac{k_xk_y}{1-2\nu(z)}v_1(z)+\frac{ik_y}{1-2\nu}v_6(z)&\\ \frac{\mu(z+\Delta z)v_6(z+\Delta z)-\mu(z-\Delta z)v_6(z-\Delta z)}{2\Delta z} =&\\ \frac{1}{1+\frac{1}{1-2\nu(z)}}\left[-(k_x^2+k_y^2)v_3(z)+\frac{ik_x}{1-2\nu(z)}v_4(z)+\frac{ik_y}{1-2\nu(z)}v_5(z)\right],&\end{aligned} \tag{16}$$

where k_x, k_y are the horizontal wavenumbers and Δz is a depth step, $v_{1,2,3}$ are Fourier-transforms of the three displacement components $u_{1,2,3}$ and $v_{4,5,6}$ are their z-derivatives. At the boundaries $z=0$ and $z=z_{\mathrm{R}}$ the central differences should be replaced with backward and forward differences (Iserles, 2008), and the boundary conditions 15 Fourier-transformed in a similar manner. In combination with the Fourier-transformed boundary conditions the above system is reduced to independent $6N_z\times 6N_z$ linear systems for finding $v_i(\Delta z_j), i=1,\ldots,6, j=1,\ldots,N_z$ for each wavenumber pair k_x, k_y, where N_z is the number of depth steps.

Solution of the above system is efficiently parallelized, with individual $6N_z\times 6N_z$ sparse systems solved independently. Furthermore, each of the systems is *banded*

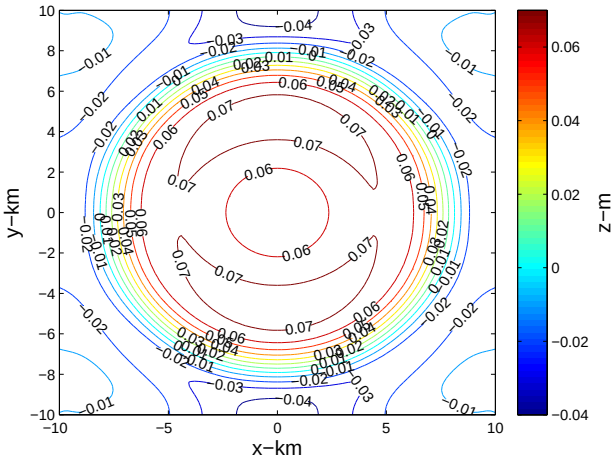

Figure 11: Contour plot of the displacements modelled from the axisymmetric pore pressure decline of Fig 2(a). [**ER**]

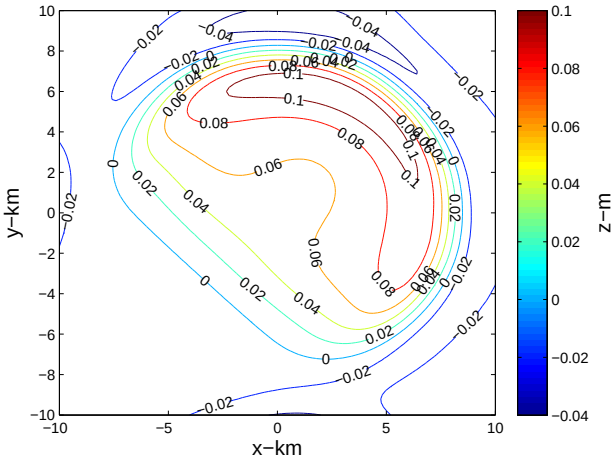

Figure 12: Contour plot of the displacements modelled from the asymmetric pore pressure decline of Fig 3(a). [**ER**]

with the bandwidth of 13 elements and therefore can be solved in a linear time and memory $O(N_z)$ (Trefethen and Bau, 1997).

Fig 11 and Fig 12 show the results of modeling surface subsidence from the axisymmetric and asymmetric pore pressure decline synthetics of Fig 2(a) and Fig 3(a). Here $N_z = 20$ with a 100 `m` depth step, the displacement field at the depth of 2 `km` was computed using operator 5. Although the above approach allows both elastic medium parameters (e.g., shear modulus μ and Poisson's ratio ν) to be vertically heterogeneous, the latter, as the ratio of the axial and transverse strains, is usually less affected by compaction, and hence we left it constant at .25. However, the depth-dependent shear modulus is given by the formula

$$\mu(z) = \frac{23\texttt{GPa}}{1. + (z_{\rm R} - z)/z_{\rm R}}. \tag{17}$$

Comparison of Fig 11 and Fig 12 with the results of Fig 2(b) and Fig 3(b) obtained above using a homogeneous model indicate larger subsidence in the heterogenous case that is consistent with a greater compliance of the overburden as determined by the heterogeneous shear modulus of equation 17.

Although depth-varying models are common in geomechanical applications, and the diffusive nature of production-induced deformation favors slowly-varying models, there exist practical applications where strong lateral heterogeneity should be taken into account (for example, in subsalt regions). The widely accepted approach to tackling such problems consists of application of the finite elements method (Iserles, 2008) to the coupled poroelastic system (Kosloff et al., 1980). While finite elements can handle arbitrary spatial heterogeneity, the main disadvantage of this approach is the necessity to solve a potentially very large system of linear equations with very sparse but generally *unstructured* matrix.

A possible extension of our approach for tackling arbitrary heterogeneity could be summarized as follows. If system 14 can be factorized

$$\begin{aligned}\nabla \cdot \mu(x_1,x_2,x_3) \left[\left(\frac{\partial u_i}{\partial x_j} + \frac{\partial u_j}{\partial x_i} \right) + \frac{2\nu}{1-2\nu} \frac{\partial u_k}{\partial x_k} \delta_{ij} \right] = \\ \left(c_1 \frac{\partial}{\partial x_3} + P_1(\frac{\partial}{\partial x_1}, \frac{\partial}{\partial x_2}) \right) \times \\ \left(c_2 \frac{\partial}{\partial x_3} + P_2(\frac{\partial}{\partial x_1}, \frac{\partial}{\partial x_2}) \right) u,\end{aligned} \tag{18}$$

where $P1$ and $P2$ are some pseudo-differential operators and c_1, c_2 are some functions, then given the boundary conditions 15, the boundary-value problem 14,15 can be solved by solving

$$\left(c_1 \frac{\partial}{\partial x_3} + P_1(\frac{\partial}{\partial x_1}, \frac{\partial}{\partial x_2}) \right) U = 0, \tag{19}$$

upward, starting from the initial condition at depth $z = z_{\mathrm{R}}$, followed by solving

$$\left(c_2 \frac{\partial}{\partial x_3} + P_2(\frac{\partial}{\partial x_1}, \frac{\partial}{\partial x_2})\right) u = U, \tag{20}$$

downward, starting from the free-surface boundary condition on the surface. Some factorisations 18 are trivial, as when the operator 20 maps the displacement field to the stress field, we effectively recover our original elastostatic system and obtain the well-known depth-extrapolation method for 6 variables (Segall, 2010). However, finding a factorisation that requires less than 6 variables *may* potentially lead to a method where the eigenmodes that correspond to exponentially increasing and decreasing solutions decouple in up and down-going extrapolation operators similar to the one-way wave equation (Claerbout, 2011). However, the author's attempts to construct linear operator factorisations 18 involving operators mapping only 3-component vector functions so far resulted in rank-deficient systems. The three displacement components may have to be complemented with an additional variable in order to achieve a pseudo-differential operator factorisation. The benefits of finding such factorisations and stable methods of solving factorized equations would extend beyond the solution of the uncoupled poroelastostatic system.

PREDICTING VELOCITY AND DENSITY CHANGES FROM DEFORMATION

Keeping in sight our ultimate objective of using geomechanical observables to regularize seismic inversion, we now turn to the question of estimating change in velocity and density due to production-induced deformation. At this point we assume that we have inverted the pore pressure decline from known subsidence and can forward-model spatial displacements in the overburden due to the pore pressure change. Given a modelled displacement field u_{123}, we can compute the strain

$$\epsilon_{ij} = \left(\frac{\partial u_i}{\partial x_j} + \frac{\partial u_j}{\partial x_i}\right) \tag{21}$$

and compute density change as

$$\Delta\rho(x_1, x_2, x_3) \approx -\rho(x_1, x_2, x_3)\epsilon_{ii}, i = 1, \ldots, 3. \tag{22}$$

Given the estimated density change 22 and strain 21, we can proceed to estimating the induced change in seismic velocities in two different but potentially complementary ways. The first approach would be to use empirical velocity-density relations (Mavko et al., 2009),(Gardner et al., 1974). However, polynomial and power-law empirical forms of Gardner's relations may produce significant errors due to the presence of cracks or flaws in the rock. While useful as an average over many rock types, the applicability of such empirical relations to estimating minute changes in pressure and

shear wave velocities at this point is moot. A more promising possibility is to use a linear empirical relation between the pressure-wave velocity and path-length change

$$\frac{dV_P}{V_P} = -R\epsilon_{33}, \tag{23}$$

where V_P is the pressure wave velocity (for normal-incidence pressure waves). While the dimensionless coefficient R in equation 23 is generally unknown, and estimates of R from empirical relations for different rock type suffer from the same kind of uncertainties as the velocity-density relations, a reasonable estimate can be obtained from observable time-shifts using the relation

$$\frac{dt}{t} = (1 + R)\epsilon_{33} \tag{24}$$

(Hatchell and Bourne, 2005). The time-shifts can be extracted from time-lapse seismic data using a cross-correlation technique similar to the one used by Hale (2009) and Ayeni (2011). We propose to use equation 24 to estimate the coefficient R where the time-shifts can be resolved, and then use the obtained value to estimate the velocity change (and time-shifts) from equations 23 and 24 where the time-lapse data has illumination gaps or is noisy.

CONCLUSION AND PERSPECTIVES

We have developed a computationally efficient method for modeling deformation from pore pressure decline and for inverting pore-pressure change from observable deformations/subsidence. The method has been implemented for both slowly-varying and layered media and tested on synthetics based on real-world examples of production-induced subsidence. We propose an approach to using observable deformations for estimating velocity change based on empirical rock-property relations.

While all the main building blocks required for regularizing time-lapse inversion with subsidence-based constrains are in place, an integrated seismic/geomechanical data set is required to validate our approach. While the deformation modeling and pore pressure inversion components can be tested on synthetic data, testing the regularization approach requires real data. Time-lapse synthetics would be generated using the same kind of techniques for modeling production-induced velocity change as we intend to use for the regularization, hence purely synthetic tests cannot completely validate our approach.

ACKNOWLEDGEMENTS

The author would like to thank Biondo Biondi for suggesting the problem of using geomechanical/geological constraints for the regularization of seismic inversion, Mark Zoback for his excellent course of reservoir geomechanics, and Paul Segall, Stewart Levin, Robert Clapp, David Nichols and Jon Claerbout for useful discussions and suggestions.

APPENDIX A

The elastostatic Green's tensor $g_i^k(x,y,z,\xi,\eta,\zeta)$ has the meaning of the displacement along axis i at point (x,y,z) due to a concentrated force along axis k at point (ξ,η,ζ). The analytical expression for the components of the Green's tensor in the elastic half-space with a free-surface boundary condition are given by the following equations (Mindlin, 1936):

$$
\begin{aligned}
g_1^1 =& w\left(\frac{3-4\nu}{r_1}+\frac{1}{r_2}+\frac{(x-\xi)}{r_1^3}+\frac{(3-4\nu)(x-\xi)^2}{r_2^3}\right)+\\
&+w\left(\frac{2(r_2^2-3(x-\xi)^2)z\zeta}{r_2^5}+\frac{4(1-\nu)(1-2\nu)(r_2^2-(x-\xi)^2-r_2(z+\zeta))}{r_2(r_2-z-\zeta)^2}\right)\\
g_2^1 =&(x-\xi)(y-\eta)w\left(\frac{1}{r_1^3}+\frac{3-4\nu}{r_2^3}-\frac{6z\zeta}{r_2^5}-\frac{4(1-\nu)(1-2\nu)}{r_2(r_2-z-\zeta)^2}\right)\\
g_3^1 =&(x-\xi)w\left(\frac{z-\zeta}{r_1^3}+\frac{(3-4\nu)(z-\zeta)}{r_2^3}-\frac{4(1-\nu)(1-2\nu)}{r_2(r_2-z-\zeta)}-\frac{6z\zeta(z+\zeta)}{r_2^5}\right)\\
g_1^2 =&g_2^1\\
g_2^2 =&w\left(\frac{3-4\nu}{r_1}+\frac{1}{r_2}+\frac{(y-\eta)}{r_1^3}+\frac{(3-4\nu)(y-\eta)^2}{r_2^3}\right)+\\
&+w\left(\frac{2(r_2^2-3(y-\eta)^2)z\zeta}{r_2^5}+\frac{4(1-\nu)(1-2\nu)(r_2^2-(y-\eta)^2-r_2(z+\zeta))}{r_2(r_2-z-\zeta)^2}\right)\\
g_3^2 =&(y-\eta)w\left(\frac{z-\zeta}{r_1^3}+\frac{(3-4\nu)(z-\zeta)}{r_2^3}-\frac{4(1-\nu)(1-2\nu)}{r_2(r_2-z-\zeta)}-\frac{6z\zeta(z+\zeta)}{r_2^5}\right)\\
g_1^3 =&(x-\xi)w\left(\frac{z-\zeta}{r_1^3}+\frac{(3-4\nu)(z-\zeta)}{r_2^3}+\frac{4(1-\nu)(1-2\nu)}{r_2(r_2-z-\zeta)}+\frac{6z\zeta(z+\zeta)}{r_2^5}\right)\\
g_2^3 =&(y-\eta)w\left(\frac{z-\zeta}{r_1^3}+\frac{(3-4\nu)(z-\zeta)}{r_2^3}+\frac{4(1-\nu)(1-2\nu)}{r_2(r_2-z-\zeta)}+\frac{6z\zeta(z+\zeta)}{r_2^5}\right)\\
g_3^3 =&w\left(\frac{3-4\nu}{r_1}+\frac{5-12\nu+8\nu^2}{r_2}+\frac{(z-\zeta)^2}{r_1^3}+\frac{(3-4\nu)(z+\zeta)^2-2z\zeta}{r_2^3}+\frac{6z\zeta(z+\zeta)^2}{r_2^5}\right)
\end{aligned}
$$

$$
\begin{aligned}
w =& \frac{1}{16\pi\mu(1-\nu)}\\
r_1 =& \sqrt{(x-\xi)^2+(y-\eta)^2+(z-\zeta)^2}\\
r_2 =& \sqrt{(x-\xi)^2+(y-\eta)^2+(z+\zeta)^2}
\end{aligned}
$$

APPENDIX B

The methods of this paper have been implemented in the author's Fortran 2003 object-oriented framework `exp_tk`. A parallelized forward-modeling and inversion

utility `PEMODEL` for modeling and inverting 3D displacements has been implemented by the author as part of this study, and as a joint exercise with applying the author's new optimisation framework to problems of geophysical imaging and computational geophysics (Maharramov, 2011). `PEMODEL` can be found at

```
EXP_TK_INSTALL_DIR/exp_tk_0.5/src/tests/poroelastic_deform
```

Source file comments contain a description of the command-line options used with the utility. Fortran F003 module `poroelastic_green.F90` implements the poroelastostatic modeling operator and its adjoint. Solution of problem 14,15 is implemented in the forward-modeling utility `ZPEMODEL`. `ZPEMODEL` can be found at

```
EXP_TK_INSTALL_DIR/exp_tk_0.5/src/tests/depth
```

Module `poroelastic_depth.F90` implements the corresponding modeling operator. Banded systems 16 are solved using LAPACK95 computational routine `gbtrs` (Barker et al., 2001) following optional equilibration to improve the stability for very sharp vertical contrasts of elastic moduli.

The framework has no external dependencies except for Intel Fortran compiler, version 12.0 or higher and Intel Math Kernel Library version 9.0 or higher. The plots of this report have been generated using Matlab from the binaries and headers output by `PEMODEL` and `ZPEMODEL`.

REFERENCES

Ayeni, G., 2011, Time-lapse seismic imaging by linearized joint inversion. Ph.D. Thesis: Stanford Exploration Project.

Barker, V. A., L. S. Blackford, J. Dongarra, J. D. Croz, S. Hammarling, M. Marinova, J. Wasniewski, and P. Yalamov, 2001, LAPACK95 User's Guide: SIAM.

Bjork, A., 1996, Numerical methods for least squares problems: SIAM.

Claerbout, J., 2011, Basic earth imaging: Stanford Exploration Project.

Danilov, V. G., V. P. Maslov, and K. A. Volosov, 1995, Mathematical modelling of heat and mass transfer processes: Springer.

Gardner, G. H. F., L. Gardner, and A. Gregory, 1974, Formation velocity and density – the diagnostic basics for stratigraphic traps: Geophysics, **39**, 770 – 778.

Geertsma, J., 1973, Land subsidence above compacting oil and gas reservoirs: SPE-AIME European Spring Meeting.

Hale, D., 2009, A method for estimating apparent displacement vectors from time-lapse seismic images: Geophysics, **74**, V99–V107. (http://link.aip.org/link/?GPY/74/V99/1).

Hatchell, P. and S. Bourne, 2005, Rocks under strain: Strain-induced time-lapse time shifts are observed for depleting reservoirs: The Leading Edge, **24**, 1222–1225. (http://link.aip.org/link/?LEE/24/1222/1).

Iserles, A., 2008, A first course in the numerical analysis of differential equations: Cambridge University Press.

Kosloff, D., R. Scott, and J. Scranton, 1980, Finite element simulation of Wilmington oil field subsidence: I. Linear modelling: Tectonophysics, **65**, 339 – 368.

Maharramov, M., 2011, Frontiers of geophysical research: Novel asymptotic and numerical methods in geophysical applications: Frontiers of Geophysical Research Proposal.

Maslov, V., 1976, Operational methods: Mir Publishers.

Maslov, V. P., 1990, Asymptotic solutions of equations with slowly varying coefficients: Séminaire Équations aux dérives partielles (dit Goulaouic-Schwartz).

Mavko, G., T. Mukerji, and J. Dvorkin, 2009, The rock physics handbook: Cambridge University Press.

Mindlin, R. D., 1936, Force at a point in the interior of a semi-infinite solid: Physics, **7**, 195–202. (http://link.aip.org/link/?JAP/7/195/1).

Segall, P., 1992, Induced stresses due to fluid extraction from axisymmetric reservoirs: Pure and Applied Geophysics, **139**, no. 3, 535–560. (http://dx.doi.org/10.1007/BF00879950).

———, 2010, Earth and volcano deformation: Princeton University Press.

Segall, P. and S. D. Fitzgerald, 1998, A note on induced stress changes in hydrocarbon and geothermal reservoirs: Tectonophysics, **289**, 117 – 128.

Segall, P., J.-R. Grasso, and A. Mossop, 1994, Poroelastic stressing and induced seismicity near the Lacq gas field, southwestern France: Journal of Geophysics Research, **99**, no. B8, 15423–15438. (http://dx.doi.org/10.1029/94JB00989).

Trefethen, L. N. and D. Bau, 1997, Numerical linear algebra: SIAM.

Wang, H., 2000, Theory of linear poroelasticity with applications to geomechanics and hydrogeology: Princeton University Press.

Zoback, M., 2010, Reservoir geomechanics: Cambridge University Press.

Zoback, M. D. and J. C. Zinke, 2002, Production-induced normal faulting in the Valhall and Ekofisk oil fields: Pure and Applied Geophysics, **159**, no. 1, 403–420. (http://dx.doi.org/10.1007/PL00001258).

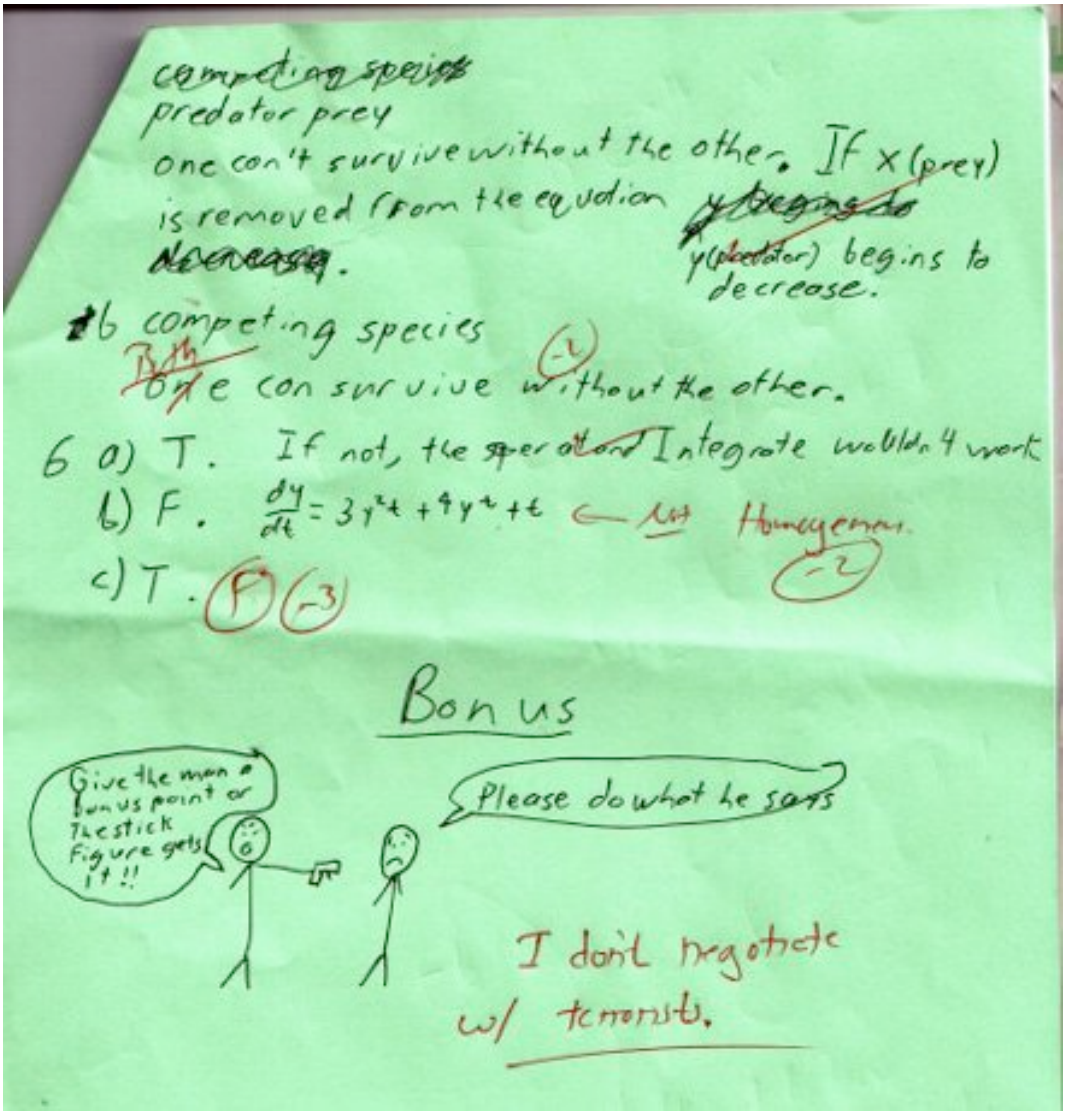
competing species
predator prey
one can't survive without the other. If x (prey) is removed from the equation y (predator) begins to decrease.
decrease.
#6 competing species
Both One can survive without the other. (-1)
6 a) T. If not, the operator Integrate wouldn't work
b) F. $\frac{dy}{dt} = 3y^2t + 4y^2 + t$ ← not Homogeneous. (-2)
c) T. (F) (-3)
Bonus
Give the man a bonus point or the stick Figure gets it!!
Please do what he says
I don't negotiate w/ terrorists.